MOLECULAR AND CELLULAR BIOLOGY, May 2001, p. 3206–3219 Vol. 21, No. 9
0270-7306/01/$04.00+0 DOI: 10.1128/MCB.21.9.3206–3219.2001

Immune System Dysfunction and Autoimmune Disease in Mice Lacking Emk (Par-1) Protein Kinase

JONATHAN B. HUROV,[1] THADDEUS S. STAPPENBECK,[2,3] CHRISTIAN M. ZMASEK,[4] LYNN S. WHITE,[1,5] SHEILA H. RANGANATH,[3] JOHN H. RUSSELL,[2] ANDREW C. CHAN,[3,5,6] KENNETH M. MURPHY,[3,5] AND HELEN PIWNICA-WORMS[1,5]*

Department of Cell Biology and Physiology,[1] Department of Molecular Biology and Pharmacology,[2] Department of Pathology and Immunology,[3] Department of Genetics,[4] Howard Hughes Medical Institute,[5] and Department of Medicine,[6] Washington University School of Medicine, St. Louis, Missouri 63110-1093

Received 22 November 2000/Returned for modification 3 January 2001/Accepted 26 January 2001

Emk is a serine/threonine protein kinase implicated in regulating polarity, cell cycle progression, and microtubule dynamics. To delineate the role of Emk in development and adult tissues, mice lacking *Emk* were generated by targeted gene disruption. *Emk*$^{-/-}$ mice displayed growth retardation and immune cell dysfunction. Although B- and T-cell development were normal, CD4^{+}T cells lacking *Emk* exhibited a marked upregulation of the memory marker CD44/pgp-1 and produced more gamma interferon and interleukin-4 on stimulation through the T-cell receptor in vitro. In addition, B-cell responses to T-cell-dependent and -independent antigen challenge were altered in vivo. As *Emk*$^{-/-}$ animals aged, they developed splenomegaly, lymphadenopathy, membranoproliferative glomerulonephritis, and lymphocytic infiltrates in the lungs, parotid glands and kidneys. Taken together, these results demonstrate that the Emk protein kinase is essential for maintaining immune system homeostasis and that loss of Emk may contribute to autoimmune disease in mammals.

Emk is a serine/threonine protein kinase with conserved homologs in yeast, worms, flies, and humans. Murine *Emk* was originally cloned by PCR using degenerate primers designed for isolating novel protein kinases (10). Emk and related family members are characterized by having a conserved amino-terminal kinase domain followed by a divergent region of unknown function and ending with a conserved region of about 100 amino acids that terminates with the sequence glutamate-leucine-lysine/asparagine-leucine. This region has been referred to as the ELKL domain, and murine Emk derived its name from ELKL motif kinase (10). Emk has also been called MARK2 (for microtubule affinity-regulating kinase 2) (7) and mPar-1 based on homology with the Par-1 protein kinase of *Caenorhabditis elegans* (4, 9). In mammals there are two additional Emk-related protein kinases, MARK1 and kp78/C-TAK1/MARK3 (7, 19, 21).

PAR-1 in both *C. elegans* and *Drosophila melanogaster* is essential for cellular polarity. In *C. elegans*, PAR-1 is required for establishment of anterior-posterior (A/P) axis formation in the one-cell embryo after fertilization (11). The PAR-1 protein localizes to the posterior cortex of the one-cell embryo and is segregated into the smaller posterior P1 cell after the first cell division in *C. elegans*, which is asymmetric (9). Mutations in *par-1* disrupt the positioning of the mitotic spindle, leading to a symmetric first division and missegregation of determinants along the A/P axis. A *Drosophila* homolog of PAR-1 has recently been reported to be essential for A/P polarization in flies (22, 25). In both *C. elegans* and *Drosophila*, the PAR-1 protein localizes to the posterior pole during the A/P axis specification. As in *C. elegans*, mutations in *Drosophila par-1* disrupt the polarized organization of the oocyte microtubule cytoskeleton and block the localization of certain posterior determinants, leading to defects both in the posterior patterning of the embryo and in the formation of germ cells. In addition to its role in regulating the microtubule cytoskeleton in the oocyte, *Drosophila par-1* is required at other stages of development (22). Interestingly, the kinase localizes to basolateral membranes of the mature follicular epithelium, perhaps suggesting a role in epithelial cell polarization (22).

The physiological functions of the EMK/PAR/MARK family of protein kinases are less clear in mammalian systems. The rat homolog of Emk (MARK2) and a related family member, MARK1, were cloned in the process of purifying protein kinases in brain extracts that phosphorylate the microtubule-associated proteins Tau, MAP2, and MAP4 in vitro. Phosphorylation of these proteins reduced their binding affinity for microtubules, resulting in microtubule destabilization (7). In addition, Emk has been localized to the basolateral membrane of cultured intestinal epithelial cells and expression of a dominant negative version of Emk causes loss of polarity (4). Taken together, these data suggest that Emk may be involved in regulation and/or maintenance of mammalian cell polarity and that this function may be facilitated via interaction with the microtubule cytoskeleton.

A third member of this family of protein kinases, C-TAK1/kp78/MARK3, phosphorylates the human Cdc25C protein phosphatase (15, 21). Cdc25C promotes mitotic entry by dephosphorylating and activating the Cdc2 protein kinase. Phosphorylation of Cdc25C by C-TAK1 occurs on serine 216 and promotes the binding of 14-3-3 proteins to Cdc25C (21). Binding of 14-3-3 proteins negatively regulates Cdc25C function by preventing it from accumulating in the nucleus. RNA interference studies of a *C. elegans* Cdc25 homologue, CDC25.1, dem-

* Corresponding author. Mailing address: Department of Cell Biology and Physiology, Washington University School of Medicine, Box 8228, 660 South Euclid Ave., St. Louis, MO 63110. Phone: (314) 362-6812. Fax: (314) 362-3709. E-mail: hpiwnica@cellbio.wustl.edu.

onstrated that the CDC25.1 protein is required for proper mitotic cleavage furrow positioning (2). Interestingly, loss of CDC25.1 function in many of the embryos causes a symmetric first division similar to that observed in *par-1* mutants.

In this study, mice lacking the Emk protein kinase were generated to elucidate the contributions made by *Emk* in developing and adult mice. In both *C. elegans* and *Drosophila*, loss of the *Emk* homolog, *par-1*, results in embryonic death. In contrast, mice lacking *Emk* were viable but exhibited embryonic and postnatal growth retardation. In addition, these mice displayed a number of immunological and anatomical defects that, taken together, are consistent with a defect in immune system homeostasis in the mouse.

MATERIALS AND METHODS

Construction of the Emk targeting vector. *Emk* genomic clones of 9.3 and 6.7 kb were isolated from a 129/SvJ mouse embryonic stem (ES) cell genomic library (BAC-4921; Genome Systems, St. Louis, Mo.) by hybridization with an isogenic 1-kb *Emk*-specific cDNA probe. Restriction enzyme maps of the *Emk* locus were determined using bacterial artificial chromosome clones and genomic DNA from NIH 3T3 L1 cells. The genomic clones contained overlapping sequences including 1.9 kb of 5′ intron sequence upstream of the first identified exon (corresponding to nucleotides 55 to 234 encoding amino acids 19 to 78). Neither clone contained the 5′-most exon(s) of the *Emk* gene. We designated the first exon contained in the genomic clones exon 2, although the 54 nucleotides encoding the first 18 amino acids of Emk may be contained in more than one exon. The genomic organization of the mouse *Emk* gene was disrupted by replacing part of exon 2 and all of exons 3 and 4 of the *Emk* gene with the pTK-neo cassette derived from pSSC9 (5). The cassette contains the neomycin phosphotransferase cDNA as a selectable marker flanked 5′ by the thymidine kinase promoter and 3′ by the thymidine kinase polyadenylation sequence.

Homologous recombination and generation of germ line chimeras. RW4 ES cells (Siteman Cancer Center at Washington University School of Medicine) were electroporated with linearized targeting vector and selected with Geneticin (G418; Gibco) (for detailed procedures, see: http://medicine.wustl.edu/~escore). A total of 126 G418-resistant ES colonies were analyzed for homologous recombination by Southern blotting using a 500-bp PCR-generated probe corresponding to a *Bam*HI-*Xba*I genomic DNA fragment at the 5′ end of the 9.3-kb genomic clone described above. Five ES clones, heterozygous for *Emk*, were injected into C57BL/6 blastocysts, which were subsequently implanted into the uteri of pseudopregnant B6C3F1 foster mothers. Male chimeras from three clones selected by agouti color were mated to C57BL/6 females. Germ line transmission was obtained for all three clones. F_1 animals were tested for the targeted *Emk* allele by Southern blotting and PCR analysis of tail DNA, using a three-primer PCR with a 5′ primer from exon 2 (5′AGCCACCTCTGCTGACGAGCAGCC), a 3′ primer from the intronic sequence between exons 2 and 3 (3′GCACCAAGTC CTGGTTCAGTCTGC), and a 3′ primer from the neomycin cassette (3′ CCT GATGCTCTTCGTCCAGATCAT). Heterozygous F_1 males and females were interbred to generate F_2 littermates.

Generation of MEFs. Mouse embryonic fibroblasts (MEFs) were derived from 13.5-day-old embryos. Following removal of the head and internal organs, embryos were rinsed with phosphate-buffered saline (PBS), minced, and digested with 1 ml of trypsin-EDTA (0.5% trypsin, 0.53 mM EDTA) per embryo for 20 min at 37°C. Trypsin was inactivated by addition of Dulbecco's minimal essential medium containing 10% fetal bovine serum, 2 mM L-glutamine, 0.1 mM nonessential amino acids, 100 μM 2-mercaptoethanol, 100 U of penicillin G per ml, and 100 μg of streptomycin per ml. Cells from single embryos were plated into one 60-mm-diameter tissue culture dish and incubated at 37°C in a 10% CO_2 humidified chamber. Cells were trypsinized and replated every 2 days. Each trypsinization and replating represented one passage. Cells were analyzed for Emk expression prior to undergoing crisis.

Emk protein analysis. A total of 2×10^6 MEFs were harvested from p60 tissue culture by tryspsinization. The cells were washed once with PBS and lysed in 300 μl of mammalian cell lysis buffer (50 mM Tris [pH 8.0], 100 mM NaCl, 2 mM dithiothreitol [DTT], 5 mM EDTA, 0.5% NP-40, 1 μM microcystin, 1 mM sodium orthovanadate, 2 mM phenylmethylsulfonyl fluoride, 0.15U of aprotinin per ml, 20 μM leupeptin, 20 μM pepstatin) at 4°C for 20 min. Various mouse tissues were homogenized in mammalian cell lysis buffer using a Fisher Scientific Powergen 700 homogenizer fitted with a sawtooth generator. After homogenization of splenic tissue, red blood cells were removed by density gradient centrifugation using Histopaque-1119 (Sigma Chemical Co.). Lysates from MEFs and whole organs were clarified by centrifugation, and protein concentrations were determined using the Bio-Rad protein assay kit. For Western blot analysis, 250-μg portions of total cellular or tissue proteins were resolved by sodium dodecyl sulfate-polyacrylamide gel electrophoresis (SDS-PAGE) (7% polyacrylamide). Western blot analysis was performed using a 1:500 dilution of affinity purified rabbit polyclonal Emk antibody (100 μg/ml) generated against a bacterially produced fusion protein of human EMK with glutathione *S*-transferase (GST-hEMK). Secondary rat anti-rabbit immunoglobulin G (IgG)–horseradish peroxidase-conjugated antibodies (Zymed) were used at a 1:2,000 dilution. An Amersham enhanced chemiluminescence detection kit was used for chemiluminography on Kodak (Rochester, N.Y.) X-OMAT AR film.

Immune complex kinase assays. A 1-mg portion of total tissue protein was incubated with 20 μl of affinity-purified Emk-specific antibody (100 μg/ml) in a volume of 550 μl for 2 h at 4°C followed by an additional hour at 4°C with 80 μl of a 50% slurry of Sepharose CL-4B–protein A beads. The beads were washed three times in mammalian cell lysis buffer and once in incomplete kinase buffer (50 mM Tris HCl [pH 7.5], 12.5 mM $MgCl_2$, 1 mM DTT) and then incubated with 1.2 μg of recombinant GST-Cdc25C(200–256) protein (20) at 30°C for 10 min in 40 μl of complete kinase buffer (50 mM Tris HCl [pH 7.5], 12.5 mM $MgCl_2$, 1 mM DTT, 50 μM ATP and 2 μCi of [γ-^{32}P]ATP [>4,000 Ci/mmol]). The reaction mixtures were adjusted to 100 mM EDTA before being boiled in SDS-PAGE sample buffer. Samples were resolved on an SDS–12% polyacrylamide gel, and proteins were visualized by Coomassie blue staining and autoradiography. ^{32}P incorporation into GST-Cdc25C motif was determined by excision of radiolabeled proteins followed by counting in a Beckman 6500 multipurpose scintillation counter.

Northern blotting. Mouse and human multiple-tissue Northern blots (Clontech) were probed for *Emk* mRNA as specified by the manufacturer. The probe used for screening mouse tissues was a PCR product of 480 bp (bp 1245 to 1725 of murine Emk) generated with the primers 5′ CCACCTCGAATTCCTACTC TAA and 3′ CTCCACTACTGCTGCTGATGTT. The probe used for screening human tissues was an 855-bp *Eco*RI restriction fragment of human *EMK* (bp 495 to 1350). The probes were labeled with [α-^{32}P]dCTP (NEN) using the Megaprime DNA-labeling system (Amersham) at 10^9 cpm/mg. The multiple-tissue Northern blot was prehybridized with ExpressHyb solution (Clontech) for 1 h at 68°C with shaking. Labeled *Emk* probe was added to 2×10^6 cpm/ml, and the blot was hybridized in ExpressHyb solution for 1 h at 68°C. The blot was then rinsed three times for 30 min at room temperature in 2X SSC (1X SSC is 0.15 M NaCl plus 0.015 M sodium citrate)–0.05% SDS. The blot was washed three times in 0.1X SSC–0.1% SDS for a total of 40 min with shaking at 50°C. The bottom half of both human and mouse multiple-tissue Northern blots was probed for human β-actin using a probe prepared as described above.

Histology, immunofluorescence, and electron microscopy. For histological studies, tissues were fixed in 10% neutral-buffered formalin, rinsed in PBS, and stored in 70% ethanol. Fixed tissues were embedded in paraffin by standard procedures. Blocks were sectioned (5 μm) and stained with hematoxylin and eosin. For electron microscopy, fresh kidney samples were sectioned into 1-mm blocks, fixed in 2% glutaraldehyde in PBS, and embedded in epoxy resin. Thin sections were stained with uranyl acetate, and electron microscopy was then performed by the Research Histology Facility, Washington University Department of Pathology.

Immunofluorescence was used to detect and localize IgG and C3 deposition within the renal parenchyma. Fresh kidneys were mounted in Tissue Tek O.C.T. compound (Sakura Finetek, Inc.), snap-frozen on dry ice, and stored at −70°C. Cryostat sections (5 μm) were cut and fixed in acetone for 20 min. The sections were washed in PBS three times for 5 min each and then preincubated with either 5% normal donkey serum (for IgG staining) or with 5% normal goat serum (for C3 staining) in PBS for 30 min. They were stained for 1 h at room temperature with a 1:100 dilution of donkey anti-mouse IgG conjugated to Cy3 (Jackson Immunoresearch) and/or with a 1:100 dilution of goat anti-mouse C3 conjugated to fluorescein (Cappel). They were washed again three times with PBS for 5 min for each were. Specimens were analyzed under an Olympus BX60 microscope.

Flow cytometry. Spleen, lymph node, and thymic tissues were homogenized in K5 medium (RPMI 1640 containing 10% fetal bovine serum, 15 mM HEPES, 10 μM nonessential amino acids, 1 mM sodium pyruvate, 2 mM L-glutamine, 50 nM 2-mercaptoethanol, 100 U of penicillin/ml, and 100 μg of streptomycin/ml) using a wire mesh. The cell suspensions were pelleted, washed twice in K5 medium, and counted using a hemacytometer. They were mixed with various monoclonal antibodies (MAbs) conjugated to either fluorescein isothiocyanate (FITC) or phycoerythrin (PE). Antibodies from PharMingen included FITC- and PE-con-

jugated anti-CD4, PE-conjugated anti-CD8, FITC- and PE-conjugated anti-CD45R/B220, PE-conjugated anti-CD44(Pgp-1), PE-conjugated anti-CD62L/MEL-14, PE-conjugated anti-CD69, PE-conjugated anti-NK1.1, PE- and FITC-conjugated anti-CD24/HSA, FITC- and PE-conjugated anti-IgM, FITC-anti-IgD, PE-conjugated anti-CD5, FITC-conjugated anti-CD90.2/Thy-1.2, FITC-conjugated anti-CD11b/MAC-1, FITC-conjugated anti-MAC-3, FITC-conjugated anti-CD3, PE-conjugated anti-CD25/IL-2Rβ, PE-conjugated anti-Ly-6G/Gr-1, PE-conjugated anti-CD138, PE-conjugated anti-Ter119, and PE-conjugated anti-CD19. All antibodies were used at 1 μg/10^6 cells after blocking nonspecific Fc binding with anti-CD16/CD32 antibody cocktail (PharMingen). Analyses were performed on a Becton Dickinson FACSCalibur instrument equipped with CellQuest software.

Purification of B- and T-cell populations. $CD4^+$ T cells and $B220^+$ B cells were purified from crude splenocyte preparations by removing red blood cells by denisty gradient centrifugation using Histopaque-1119 followed by staining with PE-conjugated anti-CD4 MAb or PE-conjugated anti-B220/CD45R MAb at 1 μg/10^6 cells. $B220^+$ B cells and $CD4^+$ T cells were then sorted using a Cytomation MoFlo cell sorter to >95% purity.

Determination of IFN-γ and IL-4 production by activated $CD4^+$ T cells. For cytokine analysis, $CD4^+$ T cells pooled from two or three mice were grown on plate-bound anti-CD3 MAb (5 μg/ml) and anti-CD28 MAb (5 μg/ml; PharMingen) for 3 days under one of three sets of conditions as indicated in the figure legends. A total of 2.5×10^5 cells were seeded into each well of a 48-well plate under Th1 development conditions containing murine recombinant interleukin-12 (rIL-12) (10 U/ml) (Genetics Institute) and anti-IL-4 MAb (10 μg/ml) (11B11) (16), under Th2 development conditions containing murine rIL-4 (100 U/ml) (from transfected P815 mastocytoma cell supernatant) and anti-IL-12 MAb (3 μg/ml) (Tosh antibody) (26), or under neutralizing conditions containing anti-IL-12 and anti-IL-4 MAbs. After 3 days, the cells were counted, replated in T175 flasks in the presence of human rIL-2 (200 U/ml) (Takeda Chemical Industries, Inc.), and expanded for four more days. Finally, on day 7, 2.5×10^5 cells were restimulated with either anti-CD3 MAb (5 μg/ml) or phorbol myristate acetate (PMA) (50 ng/ml) and ionomycin (1 μM) or concanavalin A (Sigma Chemical Co.) for 48 h in 96-well plates. Culture supernatants were then used for gamma interferon (IFN-γ) and IL-4 enzyme-linked immunosorbent assays (ELISAs).

Proliferation assays. Proliferation assays were performed with crude splenocytes or with purified populations of $CD4^+$ T cells and $B220^+$ B cells. A total of 2×10^5 cells were plated in each well of a 96-well Costar tissue culture dish and incubated for the indicated times. B-cell mitogens included goat anti-mouse IgM $F(ab')_2$ (Jackson ImmunoResearch) used at a final concentration of 20 μg/ml, anti-mouse CD40 (PharMingen) (1 μg/ml final concentration), and PMA-ionomycin (100 ng/ml and 1 μM final concentration, respectively), unless otherwise stated. Lipopolysaccharide and concanavalinA (Sigma Chemical Co.) were used in proliferation assays at concentrations of 50 and 5 μg/ml, respectively, unless otherwise indicated. All experiments were done in triplicate. The cells were incubated with 2 μCi of [^{3}H]thymidine per well (10 μCi/ml final concentration) during the final 8 h of culture. They were harvested using a Skatron Instruments Micro96Harvester and counted using a Beckman 6500 multipurpose scintillation counter.

Humoral immune responses. Retroorbital bleeds were obtained from wild-type and $Emk^{-/-}$ littermates prior to injection with either the T-cell-dependent antigen 4-hydroxy-3-nitrophenyl acetyl–keyhole limpet hemocyarin (NP-KLH) (Biosearch Tech., Inc.) or the T-cell-independent antigen NP-Ficoll (Biosearch Tech., Inc.). Mice were injected intraperitoneally with either 10 μg of NP-KLH or 20 μg of NP-ficoll. For NP-KLH, a second bleed was taken on day 10 postinjection and a second injection was given on day 14. A third bleed was taken from NP-KLH-injected mice 7 days after the second injection (21 days after the initial injection). For NP-Ficoll, a second bleed was taken on day 7 after the first injection followed by a second injection on day 10. A third bleed was taken 7 days after the second injection (17 days after the initial injection). Titers of NP-specific antibodies from serum samples were determined by ELISA. Immulon 4 HBX plates (96 wells) (Dynex Tech., Inc.) were coated with 1 μg of NP-bovine serum albumin (Biosearch Tech., Inc.) per ml. Serum samples were bound to the plates in a dilution series ranging from 1:50 to $1:3 \times 10^6$. NP-specific antibodies were then bound to biotin-conjugated goat anti-mouse Ig isotype antibodies (anti-IgM, anti-IgG1, anti-IgG2a, and anti-IgG3) from CalTag, Inc. Streptavidin-conjugated horseradish peroxidase was then used for detection of biotin-Ig with 2,2′-azino-di(3-ethylbenzthiazolinesulfonate) (ABTS) substrate. Titers of Ig from individual mice were obtained by determining the dilution at which serum samples gave optical density readings at 414 nm of 0.2 over background. The statistical significance of differences was calculated using log values of titers in a Student *t* test. Levels of NP-specific IgG were not significant prior to injection (day 0).

RESULTS

Targeted disruption of the *Emk* gene. Genomic clones of the murine *Emk* gene obtained from a 129/SvJ mouse ES cell library were used for construction of the pKOEMK1-*neo* targeting construct (Fig. 1A). pKOEMK1-*neo* removes part of exon 2 and all of exons 3 and 4 from the endogenous mouse *Emk* gene by homologous recombination. Exons 2 and 3 encode conserved residues in the small lobe of protein kinases, including the glycine-rich motif, that contributes to MgATP binding (12). Southern blot and PCR analyses indicated that ~50% of the offspring produced by chimeric males were heterozygous for the targeted mutation of the *Emk* locus. Mice from three independent targeted ES cell lines were separately bred to homozygosity for the disrupted *Emk* gene. The phenotypes described for null mice were observed in all three lineages.

Heterozygous mice were used to generate an F_2 generation of 398 mice which were genotyped by PCR (Fig. 1B) and Southern blot analysis (data not shown). The following ratios of offspring in the F_2 generation were observed at 3 weeks of age: 74 (19%) $Emk^{-/-}$, 176 (47%) $Emk^{+/-}$, and 148 (34%) $Emk^{+/+}$. The numbers of $Emk^{-/-}$ mice were slightly below the expected Mendelian value of 25%. Using a large sample Z test for statistical comparison, the number of $Emk^{-/-}$ mice observed was significantly smaller than expected, with a significance level, α, of 0.005. In addition, $Emk^{-/-}$ mice were ~25 to 30% smaller, based on weight, than their wild-type littermates from day 13.5 of embryogenesis and throughout adulthood (data not shown). Although both male and female mice lacking *Emk* were fertile, the litter size was smaller than expected when females lacking *Emk* were bred with wild-type males (data not shown).

Western blotting (Fig. 1C) and kinase reactions (Fig. 1D) demonstrated that the targeted disruption of *Emk* produces a null allele of the locus. MEFs derived from wild-type and knockout mouse embryos were generated and assayed for the presence of Emk by Western blotting using an affinity-purified antibody specific for Emk (Fig. 1C). Two electrophoretic forms of Emk were detected in MEFs derived from wild-type (lane 2) and heterozygous (lane 3) embryos. The 80- and 75-kDa forms of Emk arise by alternative splicing (8). Both electrophoretic forms of Emk were absent in MEFs derived from knockout embryos (lane 4). Next, homogenates of testis and brain derived from mice that were wild type, heterozygous, or null for *Emk* were prepared (Fig. 1D). Emk was immunoprecipitated, and kinase assays were performed in vitro using GST-Cdc25C (200–256) as a substrate. We previously demonstrated that one of the Emk-related kinases, C-TAK1, phosphorylates human Cdc25C on serine 216 (20) and confirmed that Emk phosphorylates the same residue (data not shown). GST-Cdc25C(200–256) contains amino acids 200 to 256 of human Cdc25C fused to GST. Immunoprecipitates of tissue extracts derived from wild-type but not null animals efficiently phosphorylated GST-Cdc25C(200–256) in vitro (Fig. 1D). Immunoprecipitates prepared from heterozygous animal tissues demonstrated reduced

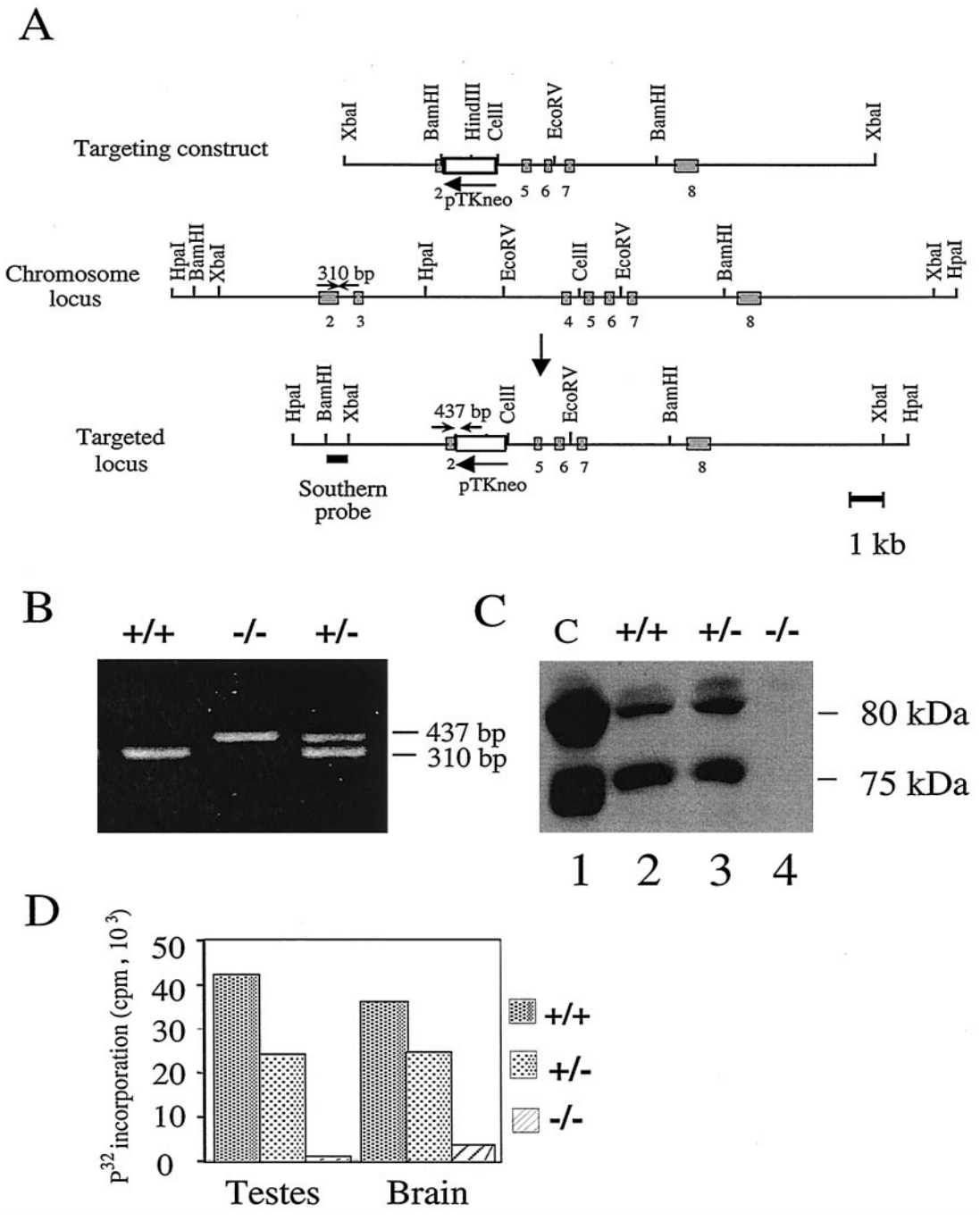

FIG. 1. Targeted disruption of the mouse *Emk* gene. (A) Structure of the targeting construct. The genomic organization of the mouse *Emk* gene was disrupted by replacing part of exon 2 and all of exons 3 and 4 of the *Emk* gene with the neomycin phosphotransferase cDNA driven by the thymidine kinase promoter (pTK-*neo*) as a selectable marker. Restriction sites in the introns flanking the targeted exons are indicated. Exons 2 to 8 are represented by shaded boxes. Small arrows depict the location of PCR primers used for genotyping. The probe used for Southern blot analysis is indicated by a bar under the targeted locus. (B) PCR analysis of genomic DNA isolated from tail clippings of F_2 *Emk* mice. $Emk^{+/+}$ mice produced a 310-bp PCR fragment, $Emk^{-/-}$ mice generated a 437-bp fragment, and $Emk^{+/-}$ mice gave rise to both products. (C) Western blot analysis of Emk protein. Lysates were prepared from 293 cells (lane 1) or from MEFs derived from $Emk^{+/+}$ (lane 2), $Emk^{+/-}$ (lane 3), or $Emk^{-/-}$ (lane 4) animals. A 250-μg portion of total cellular protein was resolved by SDS-PAGE, and Western blotting was performed using affinity-purified Emk antibody. Endogenous Emk is expressed as two alternatively spliced mRNAs encoding protein products of ~75 and 80 kDa. (D) Immune complex kinase assays. Homogenates of testis and brain were prepared from $Emk^{+/+}$, $Emk^{+/-}$, and $Emk^{-/-}$ mice. Emk was immunoprecipitated using 2.5 mg of total tissue protein, and kinase assays were performed in vitro using GST-Cdc25C(200–256) as a substrate. Proteins were resolved by SDS-PAGE, and radiolabeled proteins were visualized by autoradiography. ^{32}P-labeled substrate was excised from the gel, and radioactivity was quantitated by Cerenkov counting.

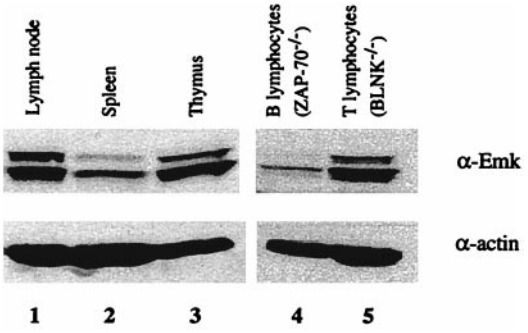

FIG. 2. Expression pattern of Emk in mouse tissues by Western blot analysis. A Western blot analysis of Emk and α-actin protein in selected lymphoid tissues and cells is shown. Enriched populations of T and B lymphocytes were isolated from the spleens of *BLNK*$^{-/-}$ and *ZAP70*$^{-/-}$ mice, respectively. The 80- and 75-kDa forms of Emk arise by alternative splicing.

ability to phosphorylate Cdc25C relative to those prepared from wild-type animal tissues.

***Emk* expression in lymphoid tissues and cells.** Northern blot analysis of various normal mouse tissues indicated that *Emk* mRNA is ubiquitously expressed with highest levels in the brain, kidneys, testes, and lungs, as reported previously (reference 3 and data not shown). Due to the unexpected finding of an immunological phenotype in *Emk*$^{-/-}$ mice (see below), we also examined murine lymhoid tissues for levels of Emk protein (Fig. 2). Western blot analysis revealed that murine Emk protein was present in the thymus, lymph nodes, and, to a lesser extent, spleen (Fig. 2, lanes 1 to 3). To further define the lymphoid cells that express Emk, Western blot analysis was performed on purified populations of T and B cells. Splenic B cells were isolated from mice lacking the ZAP-70 tyrosine kinase, and splenic T cells were isolated from mice lacking BLNK. ZAP-70-deficient mice have defects in T-cell development, and therefore >90% of their spleen lymphocytes are B cells (14). Conversely, BLNK-deficient mice have impaired B-cell development and >90% of their spleen lymphocytes are T cells (17). As seen in Fig. 2, Emk protein was detected in both T and B cells (lanes 4 and 5).

Normal development and impaired T-cell function in *Emk*$^{-/-}$ mice. Due to the relatively high level of Emk expression in T cells, we examined T-cell development and function in *Emk*$^{-/-}$ mice. Fluorescence-activated cell sorter (FACS) analysis using the T-cell markers Thy1, CD4, and CD8 indicated that thymic T-cell development was normal in *Emk*$^{-/-}$ mice (Table 1 and data not shown). In addition, the percentages of total CD4$^+$ and CD8$^+$ T cells were similar in the spleens and superficial inguinal lymph nodes of 8-week-old wild-type and null animals (Table 1). Although T-cell development was normal in mice lacking *Emk*, FACS analysis revealed differences in cell surface expression levels of the memory markers CD44 (Pgp-1) and CD62L (Mel-14) on CD4$^+$ T cells isolated from wild-type and null animals. CD44-low cells showed a 2.5-fold increase in CD44 expression, bringing them to a level intermediate between that of CD44-low and CD44-high cells. This was the case in CD4$^+$ splenic T cells in 12 of 13 *Emk*$^{-/-}$ mice examined at 6 to 10 weeks of age (Fig. 3A). CD44 was also found to be upregulated in CD4$^+$ T cells isolated from the lymph nodes of eight of eight *Emk*$^{-/-}$ mice examined at 6 to 10 weeks of age (Fig. 3B). Downregulation of CD62L was observed in CD4$^+$ splenic T cells in three of eight *Emk*$^{-/-}$ mice (data not shown). No differences were observed in the cell surface expression of either the IL-2 receptor α-chain (CD25) or the very early activation marker, CD69 (data not shown). These results indicate that CD4$^+$ T cells from mice lacking *Emk* express elevated levels of memory markers relative to their wild-type counterparts.

The role of *Emk* in T-cell function was determined by measuring proliferative responses and cytokine production after T-cell receptor (TCR) cross-linking in vitro. CD4$^+$ splenic T cells isolated from 8-week-old *Emk*$^{-/-}$ and wild-type mice showed similar proliferative responses to either anti-CD3 or anti-CD3 plus anti-CD28 stimulation (Fig. 3C). However, *Emk*$^{-/-}$ splenocytes activated with concanavalin A or with anti-CD3 antibody produced ~threefold more IFN-γ than did *Emk*$^{+/+}$ splenocytes after 3 days in culture (data not shown). To distinguish whether there was a specific effect in Th differentiation, we measured IFN-γ and IL-4 production in T cells that were induced to differentiate into Th1 or Th2 cells. CD4$^+$ splenic T cells stimulated with anti-CD3 and anti-CD28 were driven to differentiate to either a Th1 or Th2 phenotype and then given a secondary stimulation with anti-CD3 (see Materials and Methods). *Emk*$^{-/-}$ Th1 cells produced threefold more IFN-γ than did wild-type controls, while *Emk*$^{-/-}$ Th2 cells produced threefold more IL-4 than did wild-type controls (Fig. 3D and E). These data suggest that there was no specific defect in Th1 or Th2 differentiation by *Emk*$^{-/-}$ T cells. No differences in IL-2 production, as measured by CTLL-2 bioassays, were observed (data not shown). The population of CD4$^+$ T cells expressing intermediate levels of CD44 may account for the increased cytokine production observed after TCR stimulation of CD4$^+$ T cells derived from mice lacking Emk.

B-cell development and function in *Emk*$^{-/-}$ mice. We next investigated B-cell development and function in *Emk*$^{-/-}$ mice. B-cell development in 8-week-old *Emk*$^{-/-}$ mice appeared normal based on the presence of similar numbers of B220$^+$ cells in the spleens (Table 1) and bone marrow (data not shown) of *Emk*$^{+/+}$ and *Emk*$^{-/-}$ mice. In addition, surface expression of IgM and IgD on splenocytes from *Emk*$^{-/-}$ animals was similar to that observed for *Emk*$^{+/+}$ mice. However, B cells lacking Emk demonstrated a consistent decrease in proliferative capacity of two- to threefold relative to cells containing wild-type levels of Emk over a wide range of anti-IgM concentrations (Fig. 4A and B). In contrast, the proliferative response of B220$^+$ splenocytes to PMA and ionomycin was unaffected by loss of Emk (Fig. 4C) whereas the proliferative response of B220$^+$ splenocytes to anti-CD40 was slightly enhanced in cells lacking Emk (Fig. 4D). Taken together, these data suggest that *Emk*$^{-/-}$ B cells have a specific defect in their proliferative response to IgM cross-linking.

Perturbed humoral immune responses in *Emk*$^{-/-}$ mice. Mice challenged with T-cell-independent antigens secrete IgM, and this is followed by a switch to IgG3 (6). To determine whether this response was altered in *Emk*$^{-/-}$ mice, animals were immunized with NP-Ficoll and the serum antibody response was measured. On day 7, the average serum IgM levels in *Emk*$^{-/-}$ mice were somewhat lower than in *Emk*$^{+/+}$ mice; however, this difference was not statistically significant (Fig.

5A). On day 17 after challenge, IgM levels in $Emk^{-/-}$ mice were on average ~4.0-fold lower than IgM levels in their $Emk^{+/+}$ littermates ($P < 0.001$). Average IgG3 levels in $Emk^{-/-}$ mice were ~3.5-fold lower than in $Emk^{+/+}$ controls ($P < 0.05$). Taken together, these data suggest a subtle defect in the ability of $Emk^{-/-}$ mice to produce both IgM and IgG3 in response to a T-cell-independent challenge. This defect may correlate with in vitro data indicating a B-cell proliferative defect in $Emk^{-/-}$ mice in response to IgM cross-linking.

Challenging mice with T-cell-dependent antigens induces the rapid secretion of low-affinity IgM antibodies in B cells, followed by a switch to secretion of IgG and, following somatic mutation, secretion of higher-affinity antibodies (1). To assess the T-cell-dependent responses of $Emk^{-/-}$ and $Emk^{+/+}$ littermates, animals were immunized with NP-KLH. Early NP-specific IgM responses were not statistically different in $Emk^{-/-}$ mice on day 10 or 21 (Fig. 5B) postinjection. However, T-cell-dependent IgG1 and IgG2a responses in $Emk^{-/-}$ mice were on average ~7.5-fold ($P < 0.005$) and ~9.5-fold ($P < 0.005$) higher, respectively, than in their $Emk^{+/+}$ littermates (Fig. 5B). Given that isotype switching to IgG1 and IgG2a in response to T-cell-dependent antigen challenge is dependent on the cytokines IL-4 and IFN-γ, respectively (18), these data correlate well with the T-cell activation assays carried out in vitro, showing elevated IL-4 and IFN-γ production by $Emk^{-/-}$ T cells relative to $Emk^{+/+}$ T cells after TCR cross-linking (Fig. 3D and E).

Late-onset immunological disorders in $Emk^{-/-}$ mice. Alterations in T- and B-cell function were observed in young mice lacking *Emk* (Fig. 3 to 5). T cells from $Emk^{-/-}$ mice displayed elevated levels of memory marker expression, and B cells exhibited reduced proliferative responses to B-cell receptor cross-linking in vitro. These observations suggested that $Emk^{-/-}$ mice might have a predisposition to immunological disorders including immunodeficiency or autoimmunity. Indeed, at 6 to 12 months of age, a number of gross and microscopic abnormalities became evident in $Emk^{-/-}$ mice that support the observation of T- and B-cell dysfunction. Splenomegaly and/or lymphadenopathy was observed in ~30% of 7- to 12-month-old $Emk^{-/-}$ mice (Tables 1 and 2). Total splenocyte counts from aged null animals with splenomegaly were on average twofold higher than those from their wild-type littermates, although $Emk^{-/-}$ mice were on average 30% smaller than their wild-type littermates (Table 1). Occasionally older mice presented with spleens up to 30 times larger, by weight and cell number, than their wild-type counterparts did. This increase in splenocyte cell number could not be accounted for by $CD4^+$, $CD8^+$, and $B220^+$ cells, since a proportionate increase in each of these cell types was not observed (Fig. 6A). Superficial inguinal lymph nodes of both young and aged $Emk^{-/-}$ mice were also on average more cellular than those of their wild-type counterparts due to increases in $B220^+$ cell numbers (Table 1).

Several cell surface markers were examined to identify the expanded cell population observed in spleens of aged $Emk^{-/-}$ animals with splenomegaly. This expanded population of cells lacked lineage markers for T cells (CD3, CD4, CD8, and Thy1), B cells (B220, IgM, IgD, CD19, CD138, and CD5), and myeloid cells (GR1, MAC-1, MAC-3, and NK1.1) (data not shown). However, a dramatic increase in the number of splenocytes

TABLE 1. Quantitation of T- and B-cell populations in immune tissues of $Emk^{+/+}$ and $Emk^{-/-}$ mice[a]

Tissue	Genotype	Total cell no. ± SD	Total no. of $CD4^+$ cells ± SD (% of total)	Total no. of $CD8^+$ cells ± SD (% of total)	Total no. of $B220^+$ cells ± SD (% of total)
7–8-wk-old mice					
Spleen	$Emk^{+/+}$	$(17.60 \pm 6.20) \times 10^7$ ($n = 9$)	(2.86 ± 1.25) (16.2) $\times 10^7$ ($n = 8$)	(1.58 ± 0.57) (8.9) $\times 10^7$ ($n = 8$)	(9.21 ± 3.89) (52.3) $\times 10^7$ ($n = 9$)
	$Emk^{-/-}$	$(12.10 \pm 5.30) \times 10^7$ ($n = 10$)	(1.85 ± 0.82) (15.3) $\times 10^7$ ($n = 8$)	(1.21 ± 0.59) (10.0) $\times 10^7$ ($n = 8$)	(5.25 ± 2.60) (43.3) $\times 10^7$ ($n = 10$)
Lymph node	$Emk^{+/+}$	$(3.50 \pm 2.00) \times 10^6$ ($n = 6$)	(1.77 ± 1.13) (50.5) $\times 10^6$ ($n = 6$)	(0.73 ± 0.53) (20.8) $\times 10^6$ ($n = 6$)	(0.61 ± 0.50) (17.4) $\times 10^6$ ($n = 6$)
	$Emk^{-/-}$	$(6.00 \pm 2.58) \times 10^6$ ($n = 7$)[1]	(2.29 ± 1.26) (38.2) $\times 10^6$ ($n = 7$)	(1.32 ± 0.60) (22.0) $\times 10^6$ ($n = 7$)	(1.53 ± 0.85) (25.5) $\times 10^6$ ($n = 7$)[2]
Thymus[d]	$Emk^{+/+}$	$(14.70 \pm 7.9) \times 10^7$ ($n = 7$)	(1.33 ± 0.96) (10.0) $\times 10^7$ ($n = 7$)	(0.45 ± 0.16) (3.4) $\times 10^7$ ($n = 7$)	
	$Emk^{-/-}$	$(13.90 \pm 6.4) \times 10^7$ ($n = 10$)	(1.27 ± 0.80) (9.1) $\times 10^7$ ($n = 8$)	(0.41 ± 0.23) (3.0) $\times 10^7$ ($n = 8$)	
7–12-m-old mice					
Spleen	$Emk^{+/+}$	$(14.82 \pm 4.98) \times 10^7$ ($n = 11$)	$(2.85 \pm 1.22) \times 10^7$ (19.2) ($n = 10$)	(1.24 ± 0.57) (8.4) $\times 10^7$ ($n = 8$)	(5.98 ± 3.55) (40.4) $\times 10^7$ ($n = 11$)
	$Emk^{-/-b}$	$(33.13 \pm 11.62) \times 10^7$ ($n = 8$)[3]	$(4.63 \pm 3.56) \times 10^7$ (14.0) ($n = 8$)	$(1.81 \pm 0.94) \times 10^7$ (5.5) ($n = 7$)	(5.09 ± 4.06) (15.4) $\times 10^7$ ($n = 8$)
	$Emk^{-/-}$	$(10.15 \pm 4.36) \times 10^7$ ($n = 8$)	$(1.98 \pm 0.92) \times 10^7$ (19.5) ($n = 6$)	$(0.92 \pm 0.38) \times 10^7$ (9.1) ($n = 5$)	(4.34 ± 2.92) (42.8) $\times 10^7$ ($n = 8$)
Lymph node	$Emk^{+/+}$	$(3.66 \pm 4.54) \times 10^6$ ($n = 9$)	$(1.67 \pm 2.31) \times 10^6$ (45.6) ($n = 6$)	ND[c]	(0.94 ± 0.81) (25.6) $\times 10^6$ ($n = 7$)
	$Emk^{-/-c}$	$(9.90 \pm 6.35) \times 10^6$ ($n = 6$)[2]	$(3.09 \pm 1.92) \times 10^6$ (31.2) ($n = 4$)	ND	(5.74 ± 4.98) (58.0) $\times 10^6$ ($n = 4$)[4]
	$Emk^{-/-}$	$(7.07 \pm 3.9) \times 10^6$ ($n = 6$)[1]	$(2.06 \pm 1.09) \times 10^6$ (29.1) ($n = 6$)	ND	(2.57 ± 1.95) (36.4) $\times 10^6$ ($n = 6$)[2]

[a] Quantitation of T- and B-cell populations in immune tissues of $Emk^{+/+}$ and $Emk^{-/-}$ mice. Cell suspensions prepared from spleen, thymus, and superficial inguipal lymph nodes were analyzed by FACS using antibodies specific for CD4, CD8, and B220. A minimum of four mice per group was analyzed (the number is shown as *n*). Numbers indicate significant differences between $Emk^{+/+}$ and $Emk^{-/-}$ mice after analysis using a Student *t* test; 1, $P < 0.10$; 2, $P < 0.05$; 3, $P < 0.005$; 4, $P < 0.025$.

[b] $Emk^{-/-}$ with splenomegaly/colorectal prolapse.

[c] ND, not done.

[d] For $CD4^+/CD8^+$ cells, values are as follows: $Emk^{+/+}$, (11.9 ± 7.00) (80.9) $\times 10^7$ ($n = 7$); $Emk^{-/-}$, (11.0 ± 5.20) (79.1) $\times 10^7$ ($n = 8$).

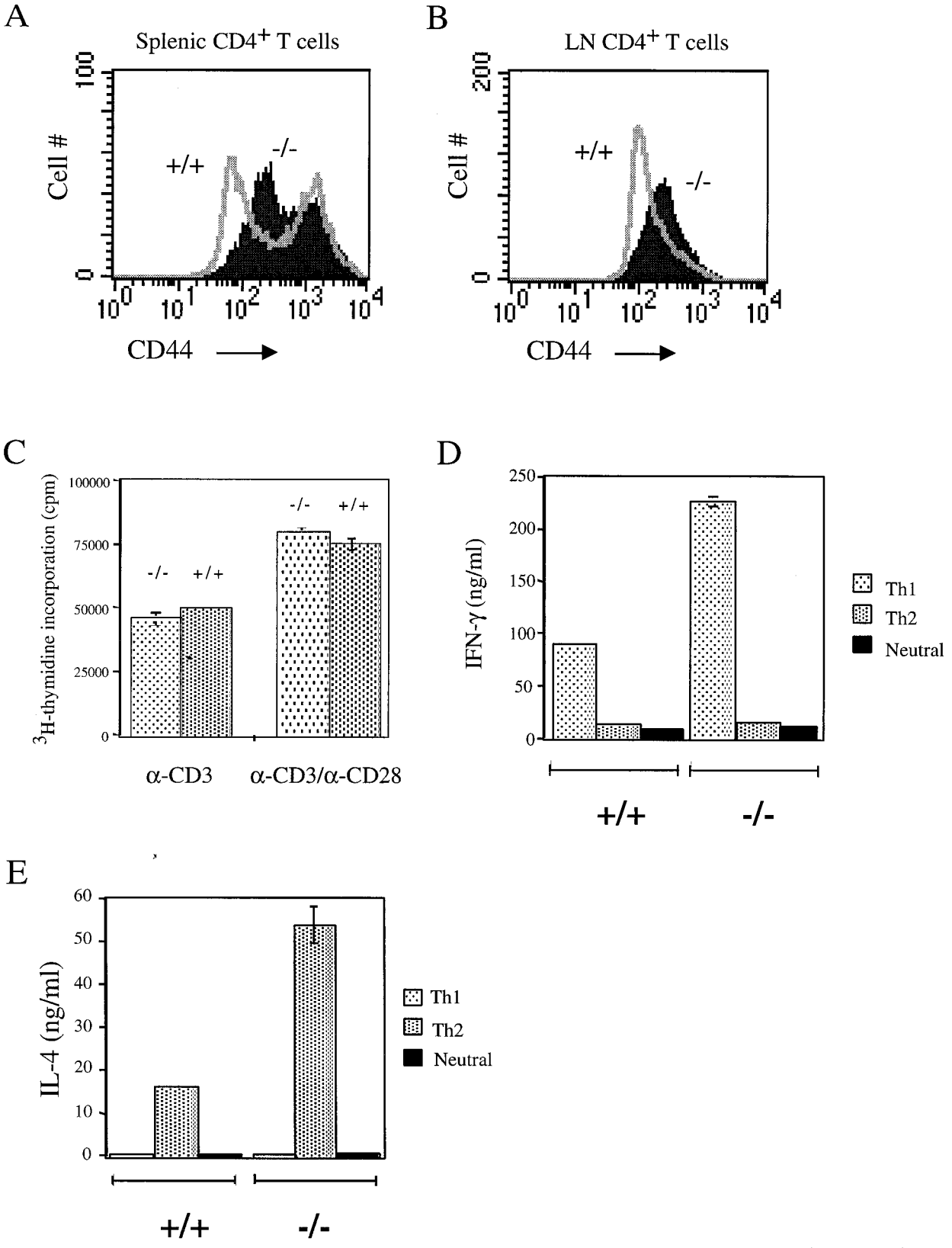

FIG. 3. Analysis of CD44 expression levels, proliferative capacity, and cytokine production in T lymphocytes of $Emk^{+/+}$ and $Emk^{-/-}$ mice. (A and B) CD44 (pgp-1) expression levels were analyzed by FACS on $CD4^+$ T cells isolated from spleens (A) and lymph nodes (B) of $Emk^{+/+}$ and $Emk^{-/-}$ mice. (C) Cell proliferation ($CD4^+$ T cells) was measured by [^{3}H]thymidine incorporation after stimulation with either anti-CD3 or anti-CD3 plus anti-CD28. Standard deviations for triplicate samples obtained from two $Emk^{+/+}$ and two $Emk^{-/-}$ mice are shown as error bars along the *y* axis. (D and E) $CD4^+$ splenic T cells pooled from two to three animals were driven to differentiate to Th1, Th2, or neutral phenotypes, and ELISAs for IFN-γ (D) or IL-4 (E) were performed as described in Materials and Methods. Each experiment was performed a minimum of three times, and standard deviations are shown as error bars along the *y* axis.

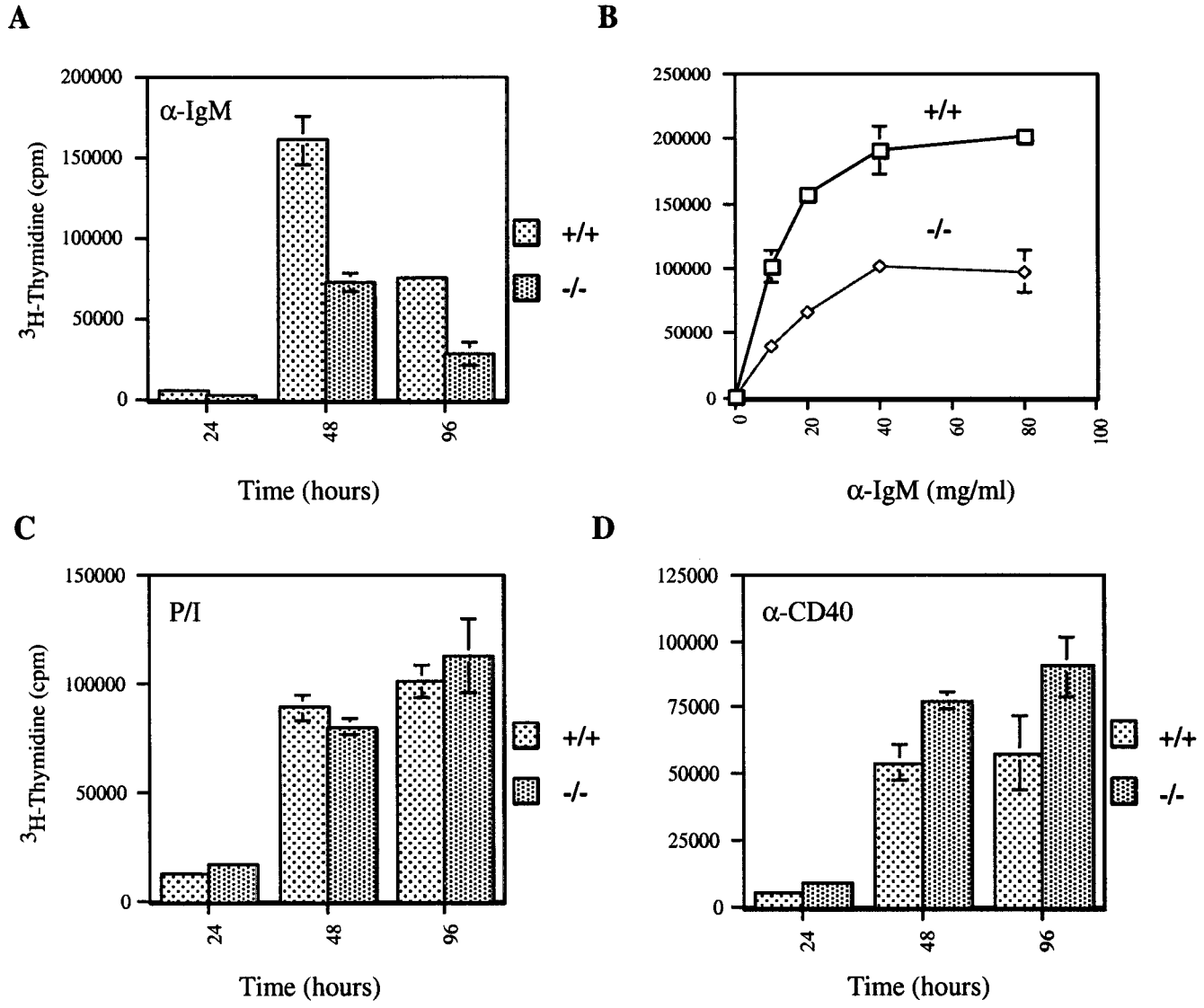

FIG. 4. Reduced B-cell proliferative capacity in $Emk^{-/-}$ mice. $B220^+$ splenocytes isolated from 8-week-old $Emk^{+/+}$ and $Emk^{-/-}$ mice were induced to proliferate by incubation with 20 μg of anti-IgM antibody per ml for the indicated times (A), with different concentrations of anti-IgM antibody (5 to 80 μg/ml) for 48 h (B), with PMA and ionomycin (C), or with anti-CD40 antibody (D). Cell proliferation was measured by [^{3}H]thymidine incorporation using pooled splenocytes from two animals per genotype, and each experiment was repeated a minimum of three times. Standard deviations for triplicate samples are shown as error bars along the *y* axis.

coexpressing the heat-stable antigen (HSA) (mouse CD24) and Ter119 (an erythroid cell lineage marker) was detected. As seen in Fig. 6B, ~11% of wild-type splenocytes were HSA Ter119 double positive. This is in contrast to the situation for aged $Emk^{-/-}$ animals with enlarged spleens, where the HSA^+ $Ter119^+$ cells represented between 20 and 80% of the total population (Fig. 6C). Forward- and side-scatter FACS analysis of the $Ter119^+$ cells indicated that these cells are nucleated (data not shown) and suggest that they are erythrocyte progenitors. $Emk^{-/-}$ spleens often displayed follicular expansion, which was due to enlargement of follicular cells rather than to increased cell numbers (data not shown).

Lymphocytic infiltrates were observed in the kidneys (Fig. 7B) and lungs (Fig. 7D) of aged $Emk^{-/-}$ mice (Table 2) but not of age-matched controls. These infiltrates consisted of a mixture of cell types including a large proportion of plasma cells and $B220^+$ cells, as observed by hematoxylin and eosin staining (Fig. 7E) and immunohistochemistry (data not shown). Lymphocytic infiltrates accumulated in both perivascular and peribronchiolar regions of the lung and in the renal cortex and medulla of the kidney. Lymphocytic infiltrates were also frequently seen in parietal salivary glands (data not shown). No evidence of vasculitis was detected in the hearts or lungs of $Emk^{-/-}$ mice. Lymphocytic infiltrates were not observed in the heart, pancreas, brain, liver, skeletal muscle, testes, or ovaries of aged mice, nor were they observed in the organs of young $Emk^{-/-}$ mice. This data suggest that although the combination of immunological disorders seen in 6 to 12-month-old individual $Emk^{-/-}$ mice was somewhat pleiotropic, perturbation of the immune system was highly penetrant in aged $Emk^{-/-}$ mu-

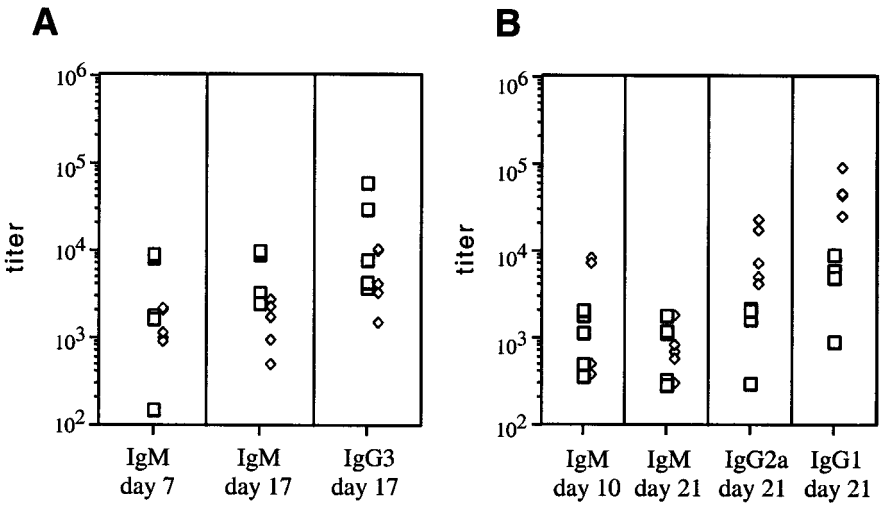

FIG. 5. The immune response of $Emk^{-/-}$ mice after challenge with T-cell-dependent and -independent antigens. $Emk^{-/-}$ (open diamonds) and $Emk^{+/+}$ (open squares) littermates (8 weeks old) were injected intraperitoneally with NP-Ficoll (A) or NP-KLH (B). Serum samples were analyzed for IgM, IgG1, IgG2a, and IgG3 by ELISA as described in Materials and Methods. The results are expressed as the dilution at which the optical density is 0.2 over background. (A) The log values of the titers were analyzed statistically. T-cell-independent IgM and IgG3 responses were ca. 4-fold lower ($P < 0.001$) and ca. 3.5-fold lower ($P < 0.05$), respectively, in $Emk^{-/-}$ mice than in their $Emk^{+/+}$ littermates after 17 days. (B) The T cell-dependent IgG2a response in $Emk^{-/-}$ mice was ca. 7.5-fold higher than that in their $Emk^{+/+}$ littermates ($P < 0.005$) after 21 days. Similarly, the IgG1 response in $Emk^{-/-}$ mice (B) was ca. 9.5-fold higher than in their $Emk^{+/+}$ littermates ($P < 0.005$).

tants. Of $Emk^{-/-}$ mice between the ages of 5 and 12 months, 85% exhibited some combination of these immunological disorders.

Proteinuria, hemoglobinuria, MPGN and colorectal prolapse in $Emk^{-/-}$ mice. The lymphoid infiltrates in the lungs, kidneys, and salivary glands of $Emk^{-/-}$ mice suggested the possibility of T- and/or B-cell dysfunction. Further evidence for this model was obtained from closer examination of kidneys from $Emk^{-/-}$ mice. Examination of aged $Emk^{-/-}$ kidneys after hematoxylin and eosin staining revealed glomeruli in $Emk^{-/-}$ mice that were markedly hypercellular and lobulated (Fig. 8B). $Emk^{-/-}$ glomeruli also showed diffuse mesangial hypercellularity and thickening of the capillary walls (Fig. 8B). This microscopic pattern is suggestive of membanoproliferative glomerulonephritis (MPGN) in humans (23). To confirm this, immunofluorescent staining of frozen kidney sections from $Emk^{+/+}$ and $Emk^{-/-}$ mice revealed that the majority of $Emk^{-/-}$ mice had significant IgG and C3 deposits that stained both capillary loops and the mesangium (Table 2; Fig. 8D to F). Finally, scanning electron microscopy of kidney sections from $Emk^{-/-}$ mice showed the presence of both subendothelial and intramembranous Ig deposits in renal capillary loops, as seen in MPGN (Fig. 8H). Scanning electron microscopy analysis also indicated the proliferation of mesangial cells, which in some cases caused capillary loop occlusion (data not shown).

Human patients with MPGN also exhibit proteinuria and mild hemoglobinuria (23). We therefore tested the mice for these two conditions. Unlike their wild-type counterparts, a significant proportion of aged $Emk^{-/-}$ mice exhibited proteinuria and/or hemoglobinuria (Table 2). Mild to severe proteinuria ($\geq$30 mg/dl) was observed in 29% of the $Emk^{-/-}$ males and 17% of the $Emk^{-/-}$ females. Only 1 of 8 $Emk^{+/-}$ males and 0 of 10 $Emk^{+/-}$ females displayed mild proteinuria. Significant hemoglobinuria (trace to 500 red blood cells/ml of urine) was also observed in 33% of $Emk^{-/-}$ males and 45% of $Emk^{-/-}$ females, while 2 of 11 and 0 of 7 $Emk^{+/-}$ females and males, respectively, exhibited hemoglobinuria.

One unexpected finding was that many of the $Emk^{-/-}$ mice with splenomegaly also presented with a colorectal prolapse (Table 2). Colorectal prolapse was seen in 20 of 67 $Emk^{-/-}$ mice (30%), 3 of 107 $Emk^{+/-}$ mice, and 0 of 85 $Emk^{+/+}$ mice. Of those aged $Emk^{-/-}$ animals with prolapse, 14 were female (14 of 34 [41%]) and 6 were male (6 of 33 [18%]), suggesting that females were more severely affected than males. Colorectal prolapse was never observed in $Emk^{-/-}$ mice younger than 5 months of age. Histological analysis of the prolapsed rectum indicated local epithelial cell proliferation with a small accumulation of neutrophils (data not shown). Absent from the colorectal prolapse was any involvement of the underlying colorectal musculature, and no other abnormalities were seen in either proximal regions of the colorectum or in more proximal regions of the intestinal tract. In addition, $Emk^{-/-}$ mice tested negative for several organisms including *Helicobacter bilus, Helicobacter hepaticus, Salmonella* spp., and *Shigella* spp. (data not shown). Thus, an inability to cope with gut flora does not appear to be cause of the colorectal prolapse, as has been observed in other immunocompromised mouse models (27). A second explanation for the appearance of the prolapse is a proliferative disorder in the colorectal epithelia of these mice, although colorectal tumors have not been observed to date.

DISCUSSION

This study describes the complex immunological phenotypes that arise in mice lacking the Emk protein kinase. Although both B- and T-cell development were normal in $Emk^{-/-}$ mice, $CD4^+$ T cells derived from spleens and lymph nodes of 8-week-old null animals expressed elevated levels of

TABLE 2. Phenotypic summary of F_2 generation mice

Mouse ID[a]	Age (mo)[a]	Sex[a]	Enlarged spleen[b]	Kidney infiltrates[c]	Lung infiltrates[c]	IgG deposits[d]	Prolapsed rectum[b]	Urine analysis[e] (protein/blood)
Emk$^{+/+}$								
171	11	M	N	+	−	+	N	ND[f]
232	11	M	N	−	−	−	N	ND
250	7	M	N	+	−	−	N	−/−
252	12	M	N	−	++	−	N	−/−
121	7	F	N	−	−	ND	N	ND
166	12	F	N	+	+	++	N	−/−
159	8	F	N	+	−	−	N	ND
242	8	F	N	−	−	−	N	ND
179	7	F	N	−	+	++	N	−/−
194	8	F	N	+	−	−	N	trace/−
253	11	F	N	−	−	ND	N	ND
254	11	F	N	−	−	+	N	ND
Emk$^{+/-}$								
170	11	M	Y	−	ND	+	Y	ND
172	11	M	Y	++	−	++	N	ND
199	12	M	N	+	+	−	N	trace/−
251	12	M	N	+	−	+	N	−/−
306	12	F	N	++	+	+++	N	−/−
173	12	F	N	++	+	++	N	trace/−
175	12	F	N	+	+	++	N	−/−
158	10		Y	++	−	++++	N	ND
Emk$^{-/-}$								
164	7	M	Y	++	++	−	Y	−/250
250	12	M	N	++	+	−	N	trace/−
293	7	M	Y	++	+	+	Y	trace/−
202	12	M	N	+++	+	++	N	30/50
212	12	F	N	+++	++	+	N	trace/−
195	12	F	N	++	+	+	N	trace/−
307	12	F	N	++++	+	++++	N	−/50
119	7	F	Y	++++	++++	ND	Y	ND
127	8	F	Y	++++	++++	++	Y	−/50
144	8	F	Y	+++	+++	++++	Y	−/250
149	7	F	Y	+++	+++	+++++	N	500/250
184	7	F	Y	+++	−	−	Y	−/250
235	8	F	Y	+	+	+	Y	−/250

[a] Mice are specified by an identification (ID) number, and their sex and age (male [M] or female [F]) are indicated.
[b] The presence (Y) or absence (N) of prolapsed rectum and enlarged spleen is indicated. Spleen enlargement was evaluated by weight and/or total splenocyte counts (see the text).
[c] Hematoxylin and eosin staining was used to detect lymphocytic infiltrates in the kidneys and lungs; − no infiltrate; +, minor infiltrate; ++++, maximal infiltrate.
[d] IgG deposition on the kidneys was determined by indirect immunofluorescence using anti-mouse IgG antibody conjugated to Cy3. Frozen kidney sections were evaluated for intensity and frequency of immunofluorescent glomeruli, and those data were used to determine a score (see Fig. 4C and D for examples of no deposition and maximal deposition, respectively); − no IgG deposition; +, minor deposition; +++++, maximal deposition.
[e] Urine was analyzed for the presence of protein (values on the left) and blood (values on the right). Protein levels range from undetectable (−) to 30–500 mg/dl, and hemoglobin levels varied from undetectable (−) to 50–250 erythrocytes/ml.
[f] Samples that were not evaluated are indicated by ND.

the cell surface memory marker CD44/pgp-1. In addition, cross-linking of the TCR on CD4$^+$ splenic T cells null for *Emk* produced higher levels of IFN-γ and IL-4 than did cross-linking of the TCR on CD4$^+$ T cells derived from wild-type littermates. Thus, CD4$^+$ T cells lacking the Emk protein kinase exhibited properties consistent with those of previously activated, memory-like T cells. In accord with these findings, *Emk*$^{-/-}$ mice also exhibited an enhanced response after challenge with the T-cell-dependent antigen NP-KLH. Elevated levels of IgG1 and IgG2a produced in *Emk*$^{-/-}$ mice after in vivo challenge may be due to enhanced help provided by *Emk*$^{-/-}$ CD4$^+$ T cells since isotype switching of B cells to IgG1 and IgG2a are IL-4- and IFN-γ-driven processes, respectively (18).

The molecular pathway by which lack of *Emk* leads to elevated levels of CD4$^+$ T cells with a phenotype typical of memory or activated cells in null animals is not known. Emk is expressed in both thymic and splenic T cells. One possibility is that Emk is required for keeping CD4$^+$ T cells in a naive state and that loss of Emk results in the inappropriate activation of these cells. In the absence of Emk, CD4$^+$ T cells may respond to self or environmental antigens. Because apoptotic cell death is an important mechanism for maintaining self-tolerance and homeostasis in the immune system, we performed antigen-induced cell death assays. Activation-induced cell death was found to be equivalent in *Emk*$^{+/+}$ and *Emk*$^{-/-}$ T cells, indicating that that the apoptotic regulatory pathway was intact in the absence of Emk (data not shown). In addition to the changes in T-cell function described above, we have observed differences in the response of B cells to activation after IgM cross-linking. The proliferative response of B220$^+$ *Emk*$^{-/-}$ splenocytes was normal in response to treatment with PMA-

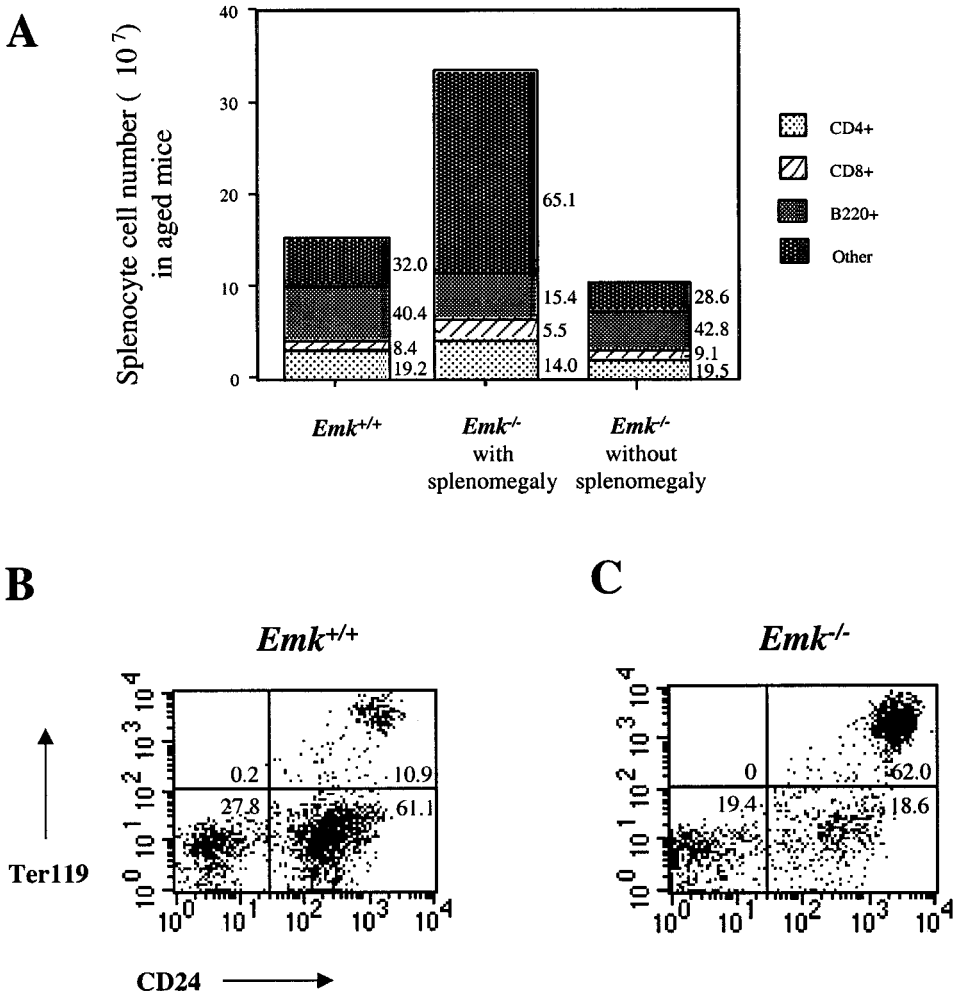

FIG. 6. Expansion of Ter119$^+$ HSA$^+$ lymphocytes in spleens of *Emk*$^{-/-}$ mice. (A) Graphical representation of the numbers of B220$^+$, CD4$^+$, and CD8$^+$ splenocytes obtained from *Emk*$^{+/+}$ and *Emk*$^{-/-}$ mice at 7 to 12 months of age (from Table 2). (B and C) Splenocytes of *Emk*$^{+/+}$ (B) and *Emk*$^{-/-}$ (C). Splenocytes isolated from mice at ~7 months of age were double stained with FITC-conjugated anti-HSA and PE-conjugated anti-Ter119. The stained cells were analyzed by flow cytometry gated on lymphocytes, and the results are shown as dot plots. The percentage of gated cells in each quadrant is indicated.

ionomycin and anti-CD40 but was reduced by ~60% relative to *Emk*$^{+/+}$ on IgM cross-linking in vitro. The finding that phorbol ester-ionomycin treatment elicits a normal proliferative response suggests that signaling downstream of protein kinase C is intact in B cells lacking *Emk*.

As *Emk*$^{-/-}$ mice aged, a number of additional phenotypes were observed. At ~6 months of age, lymphocytic infiltrates were observed in the lungs, kidneys, and salivary glands of *Emk*$^{-/-}$ mice. The majority of lymphocytic infiltrates seen in the kidneys and lungs were B220$^+$ cells and plasma cells. Superficial inguinal lymph nodes of both young and aged *Emk*$^{-/-}$ mice were on average more cellular than their wild-type counterparts, and this increase was attributable to increases in B220$^+$ cells. In addition, ~30% of *Emk*$^{-/-}$ mice developed splenomegaly at 6 to 7 months of age. B220$^+$ populations decreased significantly in enlarged *Emk*$^{-/-}$ spleens in spite of the increase in total nucleated cells. One possible explanation for the observed decline in the number of splenic B220$^+$ cells may be the exhaustive activation and differentiation of *Emk*$^{-/-}$ B cells to plasma cells (which do not express B220 on their cell surface) as a result of chronic T-cell activation. Similar observations have been observed in IL-2Rβ$^{-/-}$ mice, where activation of CD4$^+$ T cells precedes the disappearance of B220$^+$ cells from the periphery (24). A dramatic increase in the number of splenocytes coexpressing HSA (mouse CD24) and Ter119 (an erythroid cell lineage marker) was observed in *Emk*$^{-/-}$ mice. The cause of the increased erythropoiesis is unclear. Interestingly, mice deficient in both *Stat5a* and *Stat5b* have T cells with an activated or memory phenotype, and as these mice age they also develop splenomegaly associated with elevated levels of Ter119$^+$ cells (13).

The finding of activated CD4$^+$ T cells and differentiated B cells in mutant mice indicated a risk for autoimmunity. In support of this, accumulation of subendothelial IgG deposits in the capillary loops of the kidney were observed in ~50% of *Emk*$^{-/-}$ mice. Both electron microscopy and standard histological analysis also revealed hypercellularity of glomeruli due to mesangial cell proliferation. Combined, these observations

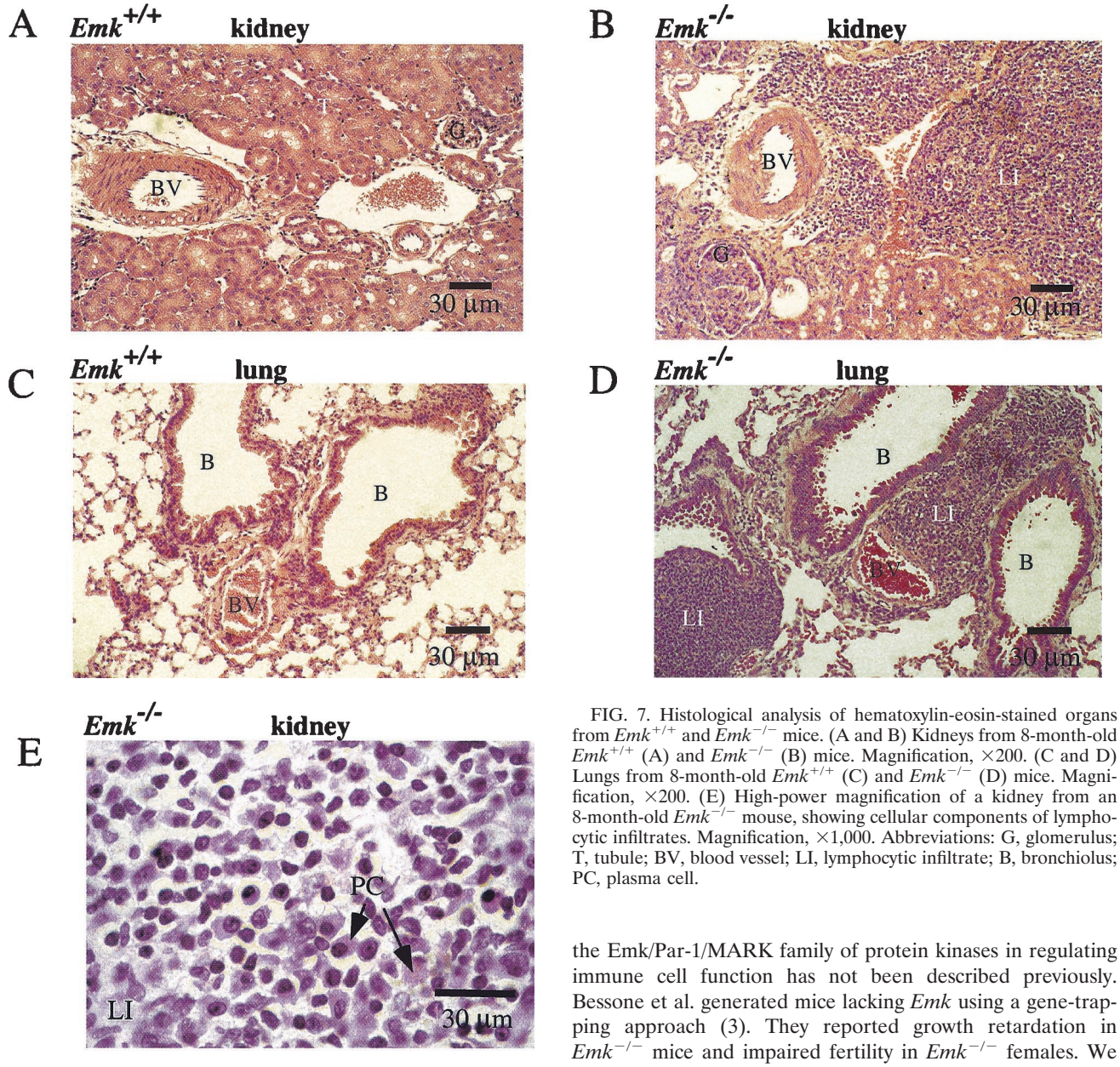

FIG. 7. Histological analysis of hematoxylin-eosin-stained organs from $Emk^{+/+}$ and $Emk^{-/-}$ mice. (A and B) Kidneys from 8-month-old $Emk^{+/+}$ (A) and $Emk^{-/-}$ (B) mice. Magnification, ×200. (C and D) Lungs from 8-month-old $Emk^{+/+}$ (C) and $Emk^{-/-}$ (D) mice. Magnification, ×200. (E) High-power magnification of a kidney from an 8-month-old $Emk^{-/-}$ mouse, showing cellular components of lymphocytic infiltrates. Magnification, ×1,000. Abbreviations: G, glomerulus; T, tubule; BV, blood vessel; LI, lymphocytic infiltrate; B, bronchiolus; PC, plasma cell.

indicate that $Emk^{-/-}$ mice develop autoimmune MPGN. Although autoimmunity could explain the phenotypes observed in $Emk^{-/-}$ mice, defects in adhesion and or homing of lymphocytes could also explain the lymphocytic infiltrates observed in the kidneys and lungs. It should also be noted that this study has not distinguished whether the immunological defects observed in $Emk^{-/-}$ mice are cell autonomous for lymphocytes. Bone marrow and organ transplants would help to distinguish whether the observed phenotypes are due to, for example, defects in antigen-presenting cells or alterations in the structural integrity of the kidneys and/or lungs. Interestingly, several of the phenotypes described in $Emk^{-/-}$ mice have also been observed with lower frequency and severity in $Emk^{+/-}$ mice, suggesting that haploinsufficiency of the Emk kinase can also lead to immune system perturbation. A role for the Emk/Par-1/MARK family of protein kinases in regulating immune cell function has not been described previously. Bessone et al. generated mice lacking *Emk* using a gene-trapping approach (3). They reported growth retardation in $Emk^{-/-}$ mice and impaired fertility in $Emk^{-/-}$ females. We have also observed growth retardation and hypofertility phenotypes in $Emk^{-/-}$ mice. However, the study by Bessone et al. (3) did not report immunological disorders in $Emk^{-/-}$ mice. This is not unexpected, in part because the major immunological disorders described here do not appear until ~6 months of age. In addition, few mice die of these disorders, and with the exception of colorectal prolapse, the other phenotypes are not visible except after histological examination of affected tissues of aged mice.

In *C. elegans* and *D. melanogaster*, the *Emk* homolog, *par-1*, acts at an early step in establishing embryonic polarity (9, 22, 25). Mammalian EMK protein has been localized to the lateral membrane domain of cultured epithelial cells, and expression of a dominant-negative version of EMK disrupts polarity of these cells, suggesting a conserved function for this family of protein kinases throughout evolution (4). However, expression of a dominant negative form of EMK also resulted in cell

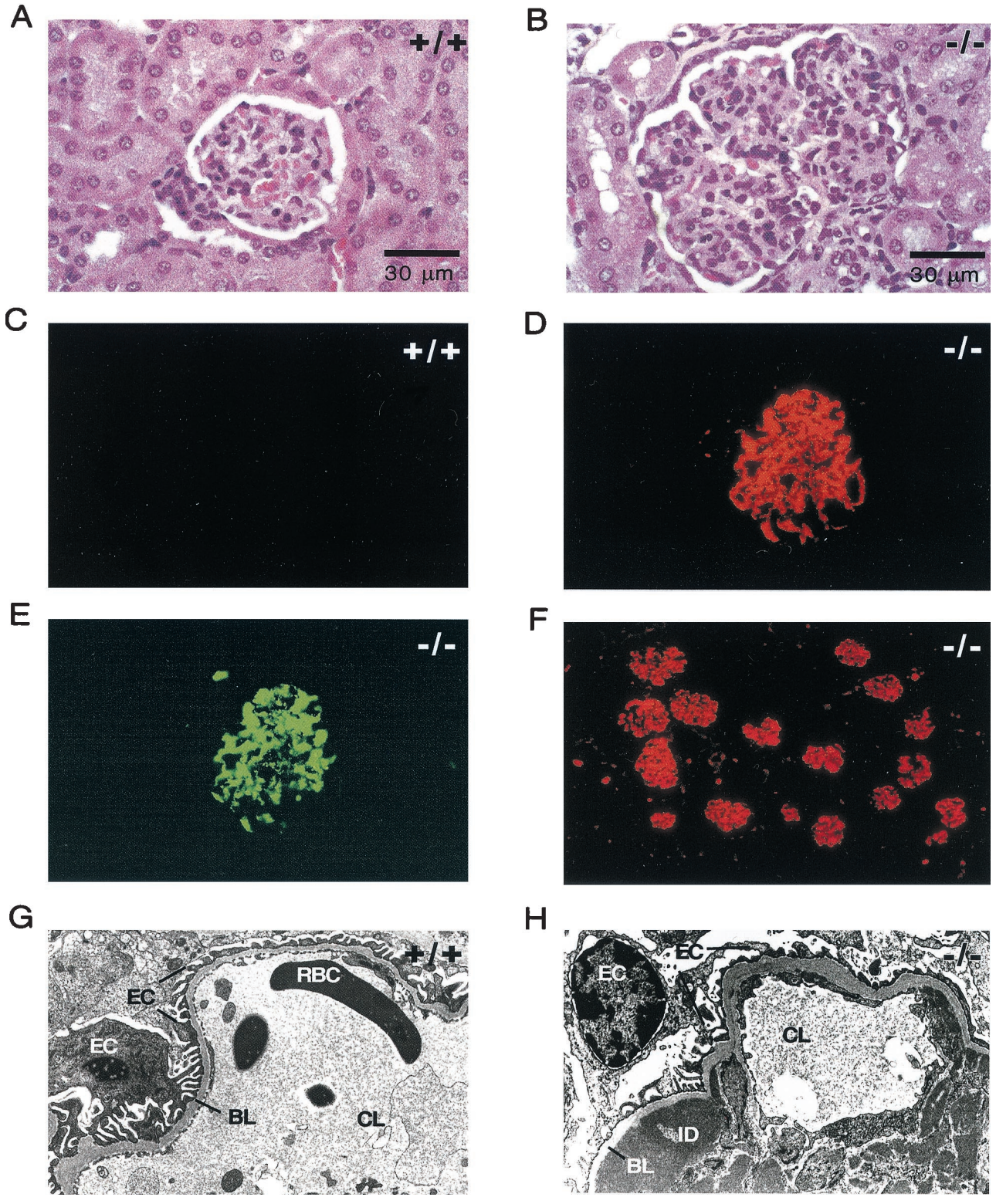

FIG. 8. $Emk^{-/-}$ mice develop autoimmune glomerulonephritis. (A and B) Glomeruli of representative $Emk^{+/+}$ (A) and $Emk^{-/-}$ (B) mice analyzed by hematoxylin and eosin staining. Magnification, ×630 (oil). (C and D) Glomeruli of representative $Emk^{+/+}$ (C) and $Emk^{+/+}$ (D) mice incubated with anti-mouse IgG coupled to Cy3 and visualized by indirect immunofluorescence. Magnification, ×400. (E) The glomerulus seen in panel D was incubated with FITC conjugated to anti-mouse C3 (anti-C3) and was visualized by direct immunofluorescence. Magnification, ×400. (F) Anti-IgG-Cy3 immunofluorescence staining of a representative $Emk^{-/-}$ kidney. Magnification, ×200. (G) Electron micrograph of an $Emk^{+/+}$ kidney capillary loop. Magnification, ×7,700. (H) Electron micrograph of $Emk^{-/-}$ kidney capillary loop. Magnification, ×10,000. Abbreviations: RBC, red blood cell; BL, basal lamina; ID, Ig deposit; CL, capillary lumen; EC, epithelial cell.

death, making it unclear from these studies whether loss of polarity was a cause or a consequence of cell death. Lymphocytes must polarize in order to form cell-cell contacts during antigen recognition and in order to migrate through endothelial cells to sites of infection. One way to monitor the polarization of T cells is to measure their ability to move toward a chemoattractant in vitro. To examine the possible contribution made by Emk to T-cell polarization, $Emk^{-/-}$ T cells were monitored for their ability to move towards the chemoattractant, stromal cell-derived factor 1. No observable differences were noted between $Emk^{+/+}$ and $Emk^{-/-}$ T cells in this assay (data not shown). However, these experiments do not rule out a possible role for Emk in polarization, since the EMK-related family members C-TAK1/MARK1 or MARK3 may functionally compensate for loss of Emk under these conditions. In summary, our results demonstrate that disruption of *Emk* leads to loss of immune system homeostasis and suggest a role(s) for the Emk protein kinase in regulating T- and B-cell functions in mice.

ACKNOWLEDGMENTS

We thank E. Unanue for help with the electron microscopy and data analysis. T. McDonnell and M. Zutter are thanked for their interpretation of tissue histology. O. Kanagawa and K Sabelko are thanked for assistance with early characterization of the immune cell phenotypes. M. LaRegina is thanked for providing pathology services, M. Dustin is thanked for help with the chemotaxis assays, and R. Schreiber is thanked for assistance with the ELISAs. A. Shaw, D. Chaplin, T. Chatilla, J. Atkinson, G. Longmore, and P. Allen are thanked for valuable discussions and input. T. Ley and members of the Division of Bone Marrow Transplantation and Stem Cell Biology at Washington University are thanked for their helpful suggestions on phenotype analysis. We thank the Siteman Cancer Center ES stem cell core at Washington University for performing the ES cell electroporations, and we thank M. White for mouse blastocyst injections and generation of chimeric mice.

This work was supported in part by a scholarship to J.H. from the Lucille P. Markey foundation. A.C.C., K.M.M., and H.P.-W. are Investigators of the Howard Hughes Medical Institute.

REFERENCES

1. **Allen, D., A. Cumano, R. Dildrop, C. Kocks, K. Rajewsky, J. Roes, F. Sablitzky, and M. Siekevitz.** 1987. Timing, genetic requirements and functional consequences of somatic hypermutation during B-cell development. Immunol. Rev. **96:**5–22.
2. **Ashcroft, N., M. Srayko, M. Kosinski, P. Mains, and A. Golden.** 1999. RNA-mediated interference of a cdc25 homolog in *Caenorhabditis elegans* results in defects in the embryonic cortical membrane, meiosis, and mitosis. Dev. Biol. **206:**15–32.
3. **Bessone, S., F. Vidal, Y. Le Bouc, J. Epelbaum, M.-T. Bluet-Pajot, and M. Darmon.** 1999. EMK protein kinase-null mice: dwarfism and hypofertility associated with alterations in the somatotrope and prolactin pathways. Dev. Biol. **214:**87–101.
4. **Bohm, H., V. Brinkman, M. Drab, A. Henske, and T. V. Kurzchalia.** 1997. Mammalian homologues of *C. elegans* polarization gene product PAR-1 are asymmetrically localized in epithelial cells and may influence their polarity. Curr. Biol. **7:**603–606.
5. **Chauhan, S., and M. Gottesman.** 1992. Construction of a new universal vector for insertional mutagenesis by homologous recombination. Gene **120:** 281–286.
6. **Coffman, R. L., D. A. Lebman, and P. Rothman.** 1993. Mechanism and regulation of immunoglobulin isotype switching. Adv. Immunol. **54:**229–270.
7. **Drewes, G., A. Ebneth, U. Preuss, E.-M. Mandelkow, and E. Mandelkow.** 1997. MARK, a novel family of protein kinases that phosphorylate microtubule-associated proteins and trigger microtubule disruption. Cell **89:**297–308.
8. **Espinosa, L., and E. Navarro.** 1998. Human serine/threonine protein kinase EMK1: genomic structure and cDNA cloning of isoforms produced by alternative splicing. Cytogenet. Cell Genet. **81:**278–282.
9. **Guo, S., and K. J. Kemphues.** 1995. par-1, a gene required for establishing polarity in *C. elegans* embryos, encodes a putative ser/thr kinase that is asymmetrically distributed. Cell **81:**611–620.
10. **Inglis, J. D., M. Lee, and R. E. Hill.** 1993. Emk, a protein kinase with homologs in yeast maps to mouse chromosome 19. Mamm. Genome **4:**401–403.
11. **Kemphues, K.** 2000. PARsing embryonic polarity. Cell **101:**345–348.
12. **Knighton, D. R., J. H. Zheng, L. F. Ten Eyck, V. A. Ashford, N. H. Xuong, S. S. Taylor, and J. M. Sowadski.** 1991. Crystal structure of the catalytic subunit of cyclic adenosine monophosphate-dependent protein kinase. Science **253:**407–414.
13. **Moriggl, R., D. J. Topham, S. Teglund, V. Sexl, C. McKay, D. Wang, A. Hoffmeyer, J. van Duersen, M. Y. Sangster, K. D. Bunting, G. C. Grosveld, and J. N. Ihle.** 1999. Stat5 is required for IL-2-induced cell cycle progression of peripheral T cells. Immunity **10:**249–259.
14. **Negishi, I., N. Motoyama, K. Nakayama, S. Senju, S. Hatakeyama, Q. Zhang, A. C. Chan, and D. Y. Loh.** 1995. Essential role for ZAP-70 in both positive and negative selection of thymocytes. Nature **376:**435–438.
15. **Ogg, S., B. Gabrielli, and H. Piwnica-Worms.** 1994. Purification of a serine kinase that associates with and phosphorylates human Cdc25C on serine 216. J. Biol. Chem. **269:**30461–30469.
16. **Ohara, J., and W. E. Paul.** 1985. Production of a monoclonal antibody to and molecular characterization of B-cell stimulatory factor-1. Nature **315:**333–336.
17. **Pappu, R., A. M. Cheng, B. Li, Q. Gong, C. Chiu, N. Griffin, M. White, B. P. Sleckman, and A. C. Chan.** 1999. Requirement for B cell linker protein (BLNK) in B cell development. Science **286:**1949–1954.
18. **Parker, D.** 1993. T cell-dependent B cell activation. Annu. Rev. Immunol. **11:**331–360.
19. **Parsa, I.** 1988. Loss of a Mr 78,000 marker in chemically induced transplantable carcinomas and primary carcinoma of human pancreas. Cancer Res. **48:**2265–2272.
20. **Peng, C.-Y., P. R. Graves, S. Ogg, R. S. Thoma, M. J. Byrnes, Z. Wu, M. Stephenson, and H. Piwnica-Worms.** 1998. C-TAK1 protein kinase phosphorylates human Cdc25C on serine 216 and promotes 14-3-3 binding. Cell Growth Differ. **9:**197–208.
21. **Peng, C.-Y., P. R. Graves, R. S. Thoma, Z. Wu, A. Shaw, and H. Piwnica-Worms.** 1997. Mitotic- and G2-checkpoint control: regulation of 14-3-3 protein binding by phosphorylation of Cdc25C on serine 216. Science **277:**1501–1505.
22. **Shulman, J. M., R. Benton, and D. St. Johnston.** 2000. The *Drosophila* homolog of C. elegans PAR-1 organizes the oocyte cytoskeleton and directs oskar mRNA localization to the posterior pole. Cell **101:**377–388.
23. **Silva, F. G.** 1998. Membranoproliferative glomerulonephritis, p. 309–368. *In* J. C. Jennette, J. L. Olson, M. M. Schwartz, and F. G. Silva (ed.), Hepinstall's pathology of the kidney, 5th ed., vol. 1. Lippincott-Raven, Philadelphia, Pa.
24. **Suzuki, H., T. Kundig, C. Furlonger, A. Wakeham, E. Timms, T. Matsuyama, R. Schmits, J. Simard, P. Ohashi, H. Griesser, T. Taniguchi, C. Paige, and T. Mak.** 1995. Deregulated T cell activation and autoimmunity in mice lacking interleukin-2 receptor β. Science **268:**1472–1476.
25. **Tomancak, P., F. Piano, V. Riechmann, K. C. Gunsalus, K. J. Kemphues, and A. Ephrussi.** 2000. A *Drosophila melanogaster* homologue of *Caenorhabditis elegans par-1* acts at an early step in embryonic-axis formation. Nat. Cell Biol. **2:**458–460.
26. **Tripp, C. S., M. K. Gately, J. Hakimi, P. Ling, and E. R. Unanue.** 1994. Neutralization of IL-12 decreases resistance to *Listeria* in SCID and C. B-17 mice. Reversal by IFNγ. J. Immunol. **152:**1883–1887.
27. **Ward, J., M. R. Anver, D. C. Haines, J. M. Melhorn, P. Gorelick, L. Yan, and J. G. Fox.** 1996. Inflammatory large bowel disease in immunodeficient mice naturally infected with *Helicobacter hepaticus*. Lab. Anim. Sci. **46:**15–20.